Journal of Materials Chemistry C

ROYAL SOCIETY OF CHEMISTRY

COMMUNICATION

View Article Online
View Journal | View Issue

Cite this: J. Mater. Chem. C, 2020, 8, 10761

Received 17th January 2020,
Accepted 3rd July 2020

DOI: 10.1039/d0tc00328j

rsc.li/materials-c

Resolving in-plane and out-of-plane mobility using time resolved microwave conductivity†

Shirsopratim Chattopadhyay, Robert S. Kokenyesi, Min Ji Hong, C Lowell Watts and John G. Labram *

The contactless characterization technique time resolved microwave conductivity (TRMC) provides a means to rapidly and unambiguously approximate carrier mobilities and lifetimes for a variety of semiconducting materials. When using a cavity-based approach however, the technique can conventionally only resolve carrier mobilities in the plane of the substrate. In solar cells, charge carriers are extracted in the direction perpendicular to the substrate, therefore it would be beneficial if one were able to evaluate the mobility in this direction also. Here we present a novel approach for resolving charge carrier mobilities in different planes within a sample. Using a range of 3D-printed sample holders, where the sample is held at various angles relative to the incident light, we are able to simultaneously resolve the mobility in the plane of the sample and out of the plane of the sample. As examples, we have studied the 3-dimensional corner-connected metal halide perovskite methylammonium lead iodide and the 2-dimensional perovskite precusor, lead iodide.

Introduction

A thorough understanding of the optoelectronic properties of semiconducting materials is of vital importance in developing and understanding efficient thin film solar cells.[1] The charge carrier mobility[2] and carrier lifetime[3] are important figures of merit to quantify the performance of a solar cell. Standard techniques to measure the charge carrier mobility of materials like Hall effect measurements,[4] space charge measurements,[5] steady-state photoconductance,[6] or Thin Film Transistor (TFT) measurements[7,8] suffer from the drawback of requiring continuous thin film growth or single crystals, which may not be always possible for new materials.[9] Additionally, electrical contacts can greatly modify the properties of semiconductors,[10,11] making a comparison between different materials dependent on the optimization of interfaces.

Contactless techniques like time resolved microwave conductivity (TRMC)[12,13] or terahertz conductivity[14] are hence valuable for the characterization of a range of semiconducting materials.[13,15–22] TRMC enables one to measure the transient photoconductivity of a sample after excitation by a pulsed optical source (typically a nanosecond pulsed laser).[23] Unlike traditional measurement techniques, TRMC does not require electrical contacts. TRMC measurements can hence be carried out on crystals,[24] thin films,[25] fluids,[26] suspensions,[27] powders,[28] or discontinuous films.[9] By default, cavity-based TRMC measurements only enable one to probe charge carrier motion in a direction parallel to the plane of the sample, although in-plane *vs.* out-of-plane measurements have been demonstrated in organic semiconductors by changing the orientation of the sample in the cavity.[29,30] Charges in solar cell devices are typically extracted vertically,[1] and hence rely on the transport properties in the direction perpendicular to the plane of the sample. In a recent report,[31] researchers at the National Renewable Energy Laboratory (NREL) demonstrated how one can modify a cavity-based TRMC system to resolve a proxy for charge carrier mobility in-plane and out-of-plane of the sample.

In this report, we discuss a novel approach to study charge transport in-plane and out-of-plane using TRMC, without modifying the cavity. Using a range of 3D-printed sample holders, we vary the angle at which our sample is held with respect to the electric field component of the standing electromagnetic wave. We are able to fit our measured TRMC data to a simple model which approximates the values of in-plane and out-of-plane photoconductance of the sample.

Experimental

Methylammonium lead iodide ($MAPbI_3$) thin films

$MAPbI_3$ thin films were fabricated by first preparing a precursor solution consisting of methylammonium iodide (CH_3NH_3I),

School of Electrical Engineering and Computer Science, Oregon State University, Corvallis, OR 97331, USA. E-mail: john.labram@oregonstate.edu

† Electronic supplementary information (ESI) available. See DOI: 10.1039/d0tc00328j

lead iodide (PbI_2) and dimethyl sulfoxide (DMSO) in a 1 : 1 : 1 molar ratio. This precursor solution was dissolved in *N*,*N*′-dimethylformamide (DMF) at 0.84 g ml^{-1}. The solution was then spin-cast onto quartz, using an anti-solvent (diethyl ether) in an ambient-pressure nitrogen glovebox. The samples were annealed at 80 °C for 15 minutes. CH_3NH_3I was purchased from Greatcell Solar and PbI_2 was purchased from Sigma Aldrich.

Lead iodide (PbI_2) thin films

A mixture of lead iodide (PbI_2) and dimethyl sulfoxide (DMSO) in a 1 : 1 molar ratio was dissolved in dimethylformamide (DMF). Films were spin-cast under atmospheric-pressure onto quartz substrates without any antisolvent. Films were then heated at 100 °C for 10 minutes to evaporate the solvent.

X-ray diffraction (XRD) experiments

X-ray diffraction (XRD) patterns were obtained using a Rigaku Ultima IV diffractometer in θ–2θ and parallel beam configuration.

Time-resolved microwave conductivity (TRMC) experiments

The time-resolved microwave conductivity (TRMC) system employed in this study is discussed in detail elsewhere[32,33] but is described briefly here for completeness. A Sivers IMA VO4280X/00 voltage-controlled oscillator (VCO) is used as the microwave source. The signal has an approximate power of 16 dBm and a tunable frequency between 8 GHz and 15 GHz. The VCO is powered with an NNS1512 TDK-Lambda constant 12 V power supply, and the output frequency is controlled by a Stahl Electronics BSA-Series voltage source. The oscillatory signal is incident on an antenna inside a WR90 copper-alloy waveguide. The microwaves emitted from the antenna pass through an isolator and an attenuator before they are incident on a circulator (Microwave Communication Laboratory Inc. CSW-3). The circulator acts as a uni-directional device in which signals entering from port 1 exit through port 2 and signals entering from port 2 exit through port 3. The incident microwaves pass through a fixed iris (6.35 mm diameter) into a sample cavity. The cavity supports a TE_{103} mode standing wave and consists of an ITO-coated glass window that allows optical access to the sample. The sample is mounted inside the cavity at a maximum of the electric-field component of the standing microwaves, using a 3D-printed polylactic acid (PLA) sample holder. Microwaves reflected from the cavity are then incident on port 2 of the circulator, exiting through port 3, directed through an isolator, and onto a zero-bias Schottky diode detector (Fairview Microwave SMD0218). The detector outputs a voltage which is linearly proportional to the amplitude of the incident microwaves. The detected voltage is amplified by a Femto HAS-X-1-40 high-speed amplifier (gain = ×100). The amplified detector voltage is measured as a function of time by a Textronix TDS 3032C digital oscilloscope. A Continuum Minilite II pulsed Nd:YaG laser is used to illuminate the sample. The laser pulse has a wavelength of 532 nm, a full width at half-maxima of approximately 5 ns and a maximum fluence incident on the sample of $\sim 10^{15}$ photons per cm^2 per pulse. An external trigger link is employed to trigger the oscilloscope before the laser fires. The photoconductance was evaluated from changes in the detector voltage using standard analysis.[9]

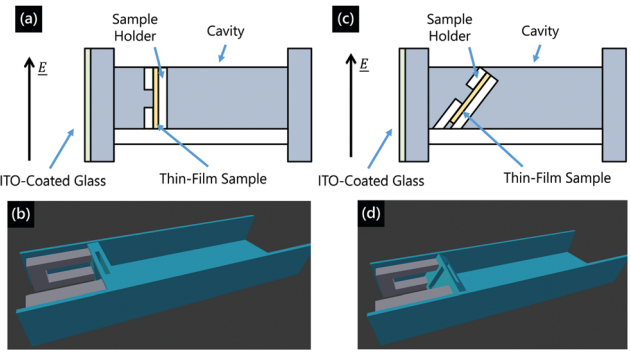

Fig. 1 (a) Schematic and (b) 3D model of sample holder for time resolved microwave conductivity (TRMC) cavity with sample aligned parallel to microwave *E*-field. In this case we can only measure the TRMC figure of merit parallel to substrate. (c) Schematic and (d) 3D model of sample holder with sample at an oblique angle to the microwave *E*-field. In this case we will measure a contribution from the mobility of carriers parallel to substrate and perpendicular to the plane of the substrate.

To change the angle of the sample relative to the electric field vector of the standing microwaves, a range of 3D-printed sample holders were made, as shown in Fig. 1. For all angles, the centre of the sample was held at a maximum of the electric field component of the standing wave. The sample holders are made from PLA, which is approximated to be transparent to microwaves for the purposes of this study.

Results and discussion

In this report we study the prototypical metal halide perovskite (MHP) methylammonium lead iodide ($MAPbI_3$), and the perovskite precursor lead iodide (PbI_2). Because $MAPbI_3$ is a 3-dimensional corner-connected perovskite[34] we anticipate the measurable mobility to be broadly isotropic. While PbI_2 is commonly used as a precursor for MHP film growth,[35] it is itself a semiconductor,[32] albeit with a larger bandgap and lower mobility than most MHPs. It is chosen here because it possesses a layered (2-dimensional) crystal structure, and it is hence anticipated to exhibit anisotropy in charge transport. While methylammonium-free[36] and mixed-cation/mixed-halide[37,38] MHP compounds are known to be more stable to environmental conditions, we here focus on $MAPbI_3$ as it remains the most well-studied and well-understood MHP compound.

Fig. S1 (ESI†) shows X-ray diffraction (XRD) spectra of thin films of $MAPbI_3$ and PbI_2. Patterns confirm the polycrystalline and textured nature of the $MAPbI_3$ and PbI_2 samples, respectively. The $MAPbI_3$ thin film exhibits the typical pattern of a polycrystalline sample when compared to the reference pattern, with no observable preferential orientation of the lattice. On the contrary, the PbI_2 thin film pattern reveals strong 00*l* peaks, consistent with preferential *c*-axis orientation of the crystal lattice normal to the substrate plane. Only minor PbI_2 peaks indicate incomplete *c*-axis alignment. It is therefore reasonable

to conclude that when the plane of the thin-film is placed at an angle of 0° relative to the electric field vector, charge carriers will travel predominantly in the PbI_2 sheets in PbI_2 thin film sample, with increasing contribution from transport between the sheets at larger incident angles. Transport in $MAPbI_3$ on the other hand is anticipated to be broadly isotropic.

During a TRMC experiment, an intense short pulse (on the order of a few nanoseconds) of photons is used to excite charge carriers in the sample *via* band-to-band transitions.[12,39] The photoconductance (ΔG) of the sample is then measured as a function of time. After the pulse concludes, ΔG decays with time. The duration and nature of the subsequent decay enables one to probe the dynamics of carrier recombination. Fig. 2 shows example TRMC transients (ΔG as a function of time) for example films of $MAPbI_3$ and PbI_2 held at various angles relative to the electric field component of the standing microwaves in the cavity.

The peak measured photoconductance (ΔG_{max}) can be used to evaluate the TRMC figure of merit: $\phi\Sigma\mu = \phi(\mu_e + \mu_h)$. ϕ is the fraction of electron–hole pairs generated per absorbed photon (between 0 and 1), μ_e is the average electron mobility and μ_h is the average hole mobility of carriers, over the illuminated sample area. $\phi\Sigma\mu$ can be evaluated using eqn (1):[9]

$$\phi\Sigma\mu = \frac{\Delta G_{max}}{\beta e I_0 F_A M} \quad (1)$$

Here, β is the ratio of the internal dimensions of the cavity, where the denominator/numerator depend on the polarization of the microwaves. In our case $\beta = 2.25$. e is the magnitude of the fundamental unit of charge. I_0 is the fluence of the laser: the number of photons that hit the surface of the sample, per unit area, per pulse. F_A is the fractional absorption of photons at the excitation wavelength ($\lambda = 532$ nm in our case) measured with ultraviolet-visible spectroscopy. M is a parameter we define as the "masking parameter" and is the fraction of the cross-sectional area of the cavity that is exposed to the incident light. In our case $M = 0.25$ for the sample held at 0° to the electric field, but as shown in Fig. 1, the value of M depends on the sample holder used. M was evaluated using simple image analysis.

$\phi\Sigma\mu$ has the same units as mobility, although carrier-type specific information is obscured. This quantity hence serves as a figure of merit for carrier mobility in the sample. Since the binding energy of $MAPbI_3$ is very low,[40,41] $\phi \approx 1$ and we can interpret $\phi\Sigma\mu$ in a similar way to how we would interpret $\Sigma\mu = \mu_e + \mu_h$. Layered compounds such as PbI_2 are anticipated to exhibit 2-dimensional properties,[42] and have a higher exciton binding energy.[43] Therefore more care must be taken when interpreting $\phi\Sigma\mu$ of such compounds. Because the carrier density in eqn (1) is implied *via* incident optical power density and absorption properties, it is not possible in general to separate out ϕ from $\Sigma\mu$ in conventional TRMC experiments. Electron based techniques[44] are able to evaluate $\Sigma\mu$ directly, but are not considered here.

Fig. 3 shows values of $\phi\Sigma\mu$ as a function of incident photon fluence for $MAPbI_3$ and PbI_2 at various angles. We have

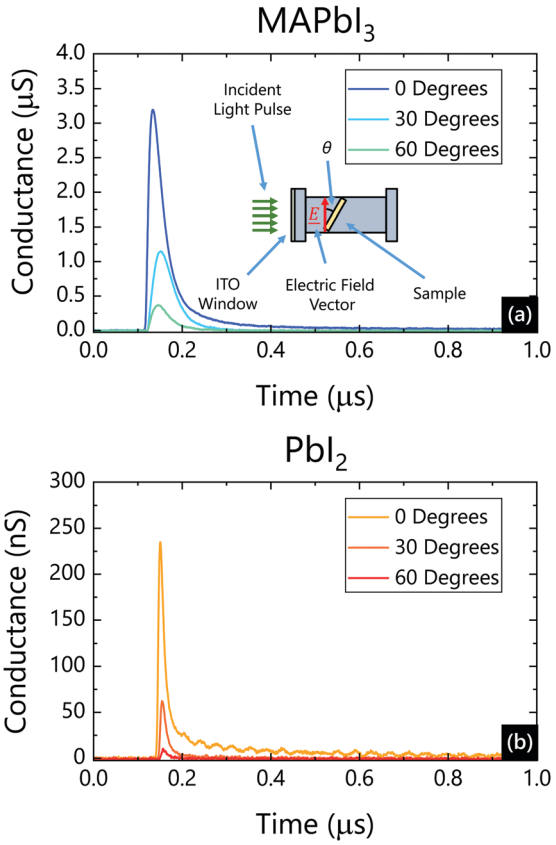

Fig. 2 Photo-induced conductance as a function of time for a thin film of (a) methylammonium lead iodide ($MAPbI_3$) and (b) lead iodide (PbI_2), measured at various angles (θ) to the electric field vector of the standing electromagnetic wave. Conductance was measured using time resolved microwave conductivity (TRMC) at room temperature in air. The incident optical fluence was 2.7×10^{14} photons per cm^2 per pulse for $MAPbI_3$ and 1.5×10^{14} photons per cm^2 per pulse for PbI_2. Inset of (a): illustration of how sample is held in microwave cavity at an angle (θ) relative to the electric field vector.

previously observed that the in-plane mobility of PbI_2 is between 1 and 2 orders of magnitude lower than that of $MAPbI_3$, which we attributed to a larger distance between transport sites in PbI_2.[32]

At high photo-generated carrier density, there is a non-negligible contribution from bimolecular and Auger recombination during the finite duration of the laser pulse.[45] This leads to a reduction in observed ΔG_{max} and, in-turn, extracted $\phi\Sigma\mu$. Models have been developed to take account of this, enabling a representative value of $\phi\Sigma\mu$ to be approximated from fluence-dependent data.[45] The lines in Fig. 3 are fits to the experimental data using this model.

Representative values of $\phi\Sigma\mu$ were approximated from 3 thin films of $MAPbI_3$ and 3 thin films of PbI_2 for various angles. Fig. 4 shows $\phi\Sigma\mu$ plotted as a function of angle for (a) $MAPbI_3$ and (b) PbI_2. The error bars represent the standard deviation between samples. The sample-to-sample variation is large as solution-processed thin films of MHPs are known to possess significant heterogeneity.[46] The standard deviation is similar to what we have observed in our lab previously.[32,33]

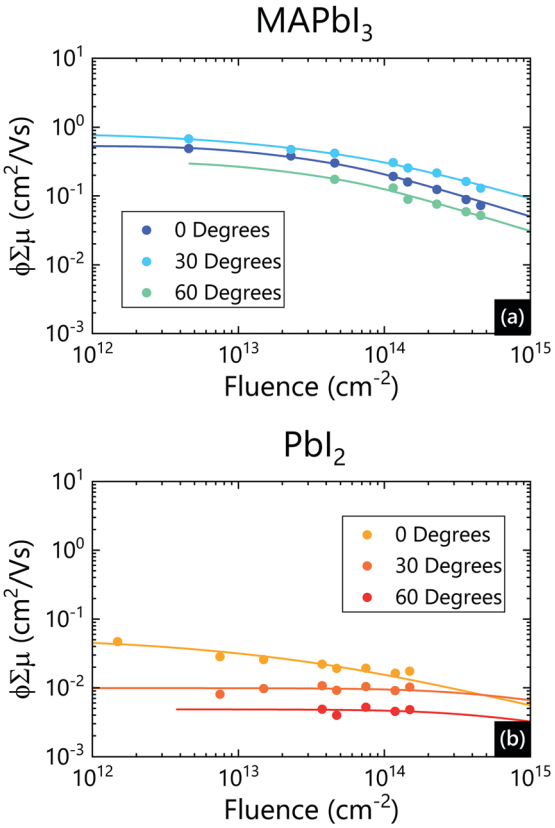

Fig. 3 Time resolved microwave conductivity (TRMC) figure of merit: $\phi\Sigma\mu = \phi(\mu_e + \mu_h)$, as a function of laser fluence for (a) methylammonium lead iodide ($MAPbI_3$) and (b) lead iodide (PbI_2), where the sample is rotated at various angles with respect to the electric field vector of the standing electromagnetic wave. Here ϕ is the fraction of electron–hole pairs generated per absorbed photon (between 0 and 1), μ_e is the average electron mobility and μ_h is the average hole mobility of carriers, over the illuminated sample area. The lines are fits to the experimental data of a model that accounts for bimolecular and Auger recombination during the finite duration of the laser pulse.[45] All measurements were carried out in air at room temperature.

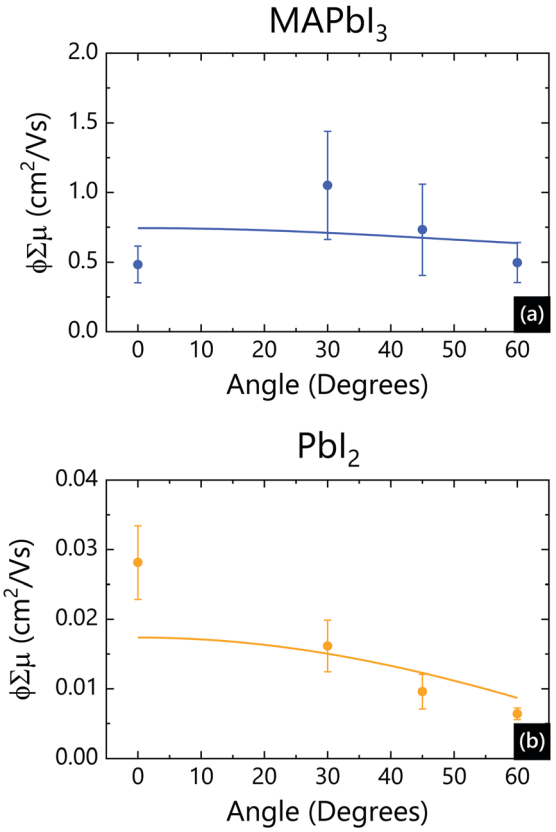

Fig. 4 Representative time resolved microwave conductivity (TRMC) figure of merit: $\phi\Sigma\mu = \phi(\mu_e + \mu_h)$, as a function of angle to the electric field vector of the standing electromagnetic wave for (a) methylammonium lead iodide ($MAPbI_3$) and (b) lead iodide (PbI_2). Here ϕ is the fraction of electron–hole pairs generated per absorbed photon (between 0 and 1), μ_e is the average electron mobility and μ_h is the average hole mobility of carriers, over the illuminated sample area. The lines are fits of eqn (2). All measurements were carried out in air at room temperature.

We can define the figure of merit in the plane of the sample as $(\phi\Sigma\mu)_\parallel$ and the figure of merit out of the plane of the sample as $(\phi\Sigma\mu)_\perp$. We interpret $(\phi\Sigma\mu)_\parallel$ and $(\phi\Sigma\mu)_\perp$ as the sum of the electron and hole mobilities, accounting for free carrier generation efficiency, when moving in each of these directions. When the sample is held at an angle of $\theta = 0^\circ$ relative to the electric field, carriers are moving in the plane of the sample, and hence the measured value of $\phi\Sigma\mu = (\phi\Sigma\mu)_\parallel$. When held at an angle $\theta \neq 0^\circ$, the carriers will be moving at an oblique angle to the plane of the sample, and hence possess contributions from both $(\phi\Sigma\mu)_\parallel$ and $(\phi\Sigma\mu)_\perp$. Using simple trigonometry, we can show that the measured $\phi\Sigma\mu$ at an angle θ to the standing electric field can be given by eqn (2):

$$\phi\Sigma\mu = \sqrt{\left[(\phi\Sigma\mu)_\parallel \cos\theta\right]^2 + \left[(\phi\Sigma\mu)_\perp \sin\theta\right]^2} \qquad (2)$$

The lines in Fig. 4 are fits of eqn (2) to the experimental data. It is clear that the fit is not perfect, but hopefully the data Illustrates that the approach in principle is valid, albeit with some variability from sample-to-sample and measurement-to-measurement variation. From these fits we extract in-plane and out-of-plane figures of merit for $MAPbI_3$ to be $(\phi\Sigma\mu)_\parallel = 0.74\ cm^2\ V^{-1}\ s^{-1}$ and $(\phi\Sigma\mu)_\perp = 0.60\ cm^2\ V^{-1}\ s^{-1}$, respectively. For PbI_2 the in-plane figure of merit was approximated to be $(\phi\Sigma\mu)_\parallel = 0.017\ cm^2\ V^{-1}\ s^{-1}$ while a fit with a non-zero value of $(\phi\Sigma\mu)_\perp$ was not possible. We hence interpret the out-of-plane figure of merit to be below our instrument resolution: $(\phi\Sigma\mu)_\perp \lesssim 10^{-4}\ cm^2\ V^{-1}\ s^{-1}$. These values agree with our initial assertion that charge transport in $MAPbI_3$ should be broadly isotropic, while in PbI_2 $(\phi\Sigma\mu)_\parallel \gg (\phi\Sigma\mu)_\perp$.

Fig. S2 (ESI†) shows TRMC measurements carried out on a powder of PbI_2 packed into a specifically designed sample holder, where the powder is held at a maximum of the electric field component of the standing wave. Because the powder has a macroscopic thickness (~mm's), we assumed the fractional absorbance was $F_A = 1$. It is expected that, unlike a thin-film, a powder measurement should probe charge carrier dynamics with a roughly angle-averaged direction. The figure of merit extracted from these measurements was $\phi\Sigma\mu = 4 \times 10^{-3}\ cm^2\ V^{-1}\ s^{-1}$, which is a factor of 2 lower than expected from the thin-film

measurement at 45° angle. However it is likely that there are significant differences in the size of crystal grains in a thin-film *vs.* a powder; a parameter known[47] to play a large role in extracted $\phi\Sigma\mu$ values.

In cavity-based TRMC, photoconductance is calculated from changes in detector voltage *via* a parameter called the sensitivity factor (K). The derivation[9,48,49] of K makes the assumption that the sample is infinitely thin, and placed at a maximum of the electric field in the cavity. Since thin films are typically ~100 nm thick and cavities are ~10 cm long, this is usually a valid assumption when the sample is held at $\theta = 0°$. However, when $\theta \neq 0°$, the sample will cover a much larger area in the electric field (not just its maximum) and this assumption is no longer valid. By integrating over the area of the sample in the cavity, it can be demonstrated (data not shown) that this would only act to underestimate the extracted value of $\phi\Sigma\mu$ by roughly 10% in the most extreme case studied ($\theta = 60°$). All values of $\Delta>G$ and $\phi\Sigma\mu$ in this report have been corrected for this phenomenon, nonetheless.

Conclusions

In conclusion, using 3D-printed sample holders we have carried out time-resolved microwave conductivity (TRMC) experiments where thin-film samples are held at an oblique angle to the electric field component of the standing electromagnetic wave. By extracting the TRMC figure of merit, $\phi\Sigma\mu$, as a function of angle, we have been able to approximate the figure of merit in the plane of the sample, $(\phi\Sigma\mu)_{\parallel}$, and out of the plane of the sample, $(\phi\Sigma\mu)_{\perp}$. By studying the 3-dimensional corner-connected semiconductor methylammonium lead iodide ($MAPbI_3$) and the layered 2-dimensional semiconductor lead iodide (PbI_2) as examples, we illustrate how the technique yields broadly expected results. The technique demonstrated in this report illustrates how TRMC can be used to elucidate the charge transport properties in semiconducting materials out of the plane of the substrate, and hence has the potential to be much more relevant for anisotropic solar-cell materials than conventional TRMC.

While previous studies[29–31] have been able to resolve in-plane and out-of-plane mobility, in this work we have been able to do so without rotating the sample by 90°. This means we do not have to modify the cavity and illuminate the sample from a different direction (*i.e.*, we can resolve both directions of mobility using the same illumination direction). By using a stepper motor and plastic rotor for example, it is clear that this approach could easily be automated, and therefore become a routine part of semiconductor evaluation. This strategy is rather general, and compatible with any thin-film system that can be studied *via* in-plane TRMC: namely a semiconductor with an optically-accessible band gap, a low background carrier concentration, and a moderate sum of hole and electron mobilities ($\gtrsim 10^{-4}$ cm^2 V^{-1} s^{-1}). While well-suited for semiconducting samples with high degrees of anisotropy such as layered metal halide compounds[9,50–52] it can equivalently be applied to organic semiconductors,[12] quantum dots,[20] chalcogenides,[17] dye-sensitized scaffolds,[18] metal oxides,[19] carbon nanotubes,[21] metal organic frameworks.[22] Additionally, there is no reason why the approach cannot be extended to study the complex conductance of semiconductors as a function of angle.[53,54]

Conflicts of interest

There are no conflicts to declare.

Acknowledgements

This work was funded by the National Science Foundation (Grant Number: 1902032).

References

1 J. Nelson, *The Physics of Solar Cells*, Imperial College Press, 2003.
2 L. M. Herz, *ACS Energy Lett.*, 2017, **2**, 1539–1548.
3 L. M. Herz, *Annu. Rev. Phys. Chem.*, 2016, **67**, 65–89.
4 Y. Chen, H. T. Yi, X. Wu, R. Haroldson, Y. N. Gartstein, Y. I. Rodionov, K. S. Tikhonov, A. Zakhidov, X.-Y. Zhu and V. Podzorov, *Nat. Commun.*, 2016, **7**, 12253.
5 P. W. M. Blom, M. J. M. de Jong and J. J. M. Vleggaar, *Appl. Phys. Lett.*, 1996, **68**, 3308–3310.
6 J. Lim, M. T. Hörantner, N. Sakai, J. M. Ball, S. Mahesh, N. K. Noel, Y.-H. Lin, J. B. Patel, D. P. McMeekin, M. B. Johnston, B. Wenger and H. J. Snaith, *Energy Environ. Sci.*, 2019, **12**, 169–176.
7 X. Y. Chin, D. Cortecchia, J. Yin, A. Bruno and C. Soci, *Nat. Commun.*, 2015, **6**, 7383.
8 J. G. Labram, D. H. Fabini, E. E. Perry, A. J. Lehner, H. Wang, A. M. Glaudell, G. Wu, H. Evans, D. Buck, R. Cotta, L. Echegoyen, F. Wudl, R. Seshadri and M. L. Chabinyc, *J. Phys. Chem. Lett.*, 2015, **6**, 3565–3571.
9 J. G. Labram, N. R. Venkatesan, C. J. Takacs, H. A. Evans, E. E. Perry, F. Wudl and M. L. Chabinyc, *J. Mater. Chem. C*, 2017, **5**, 5930–5938.
10 S. M. Sze and K. K. Ng, *Physics of Semiconductor Devices*, John Wiley & Sons, 2006.
11 P. Schulz, D. Cahen and A. Kahn, *Chem. Rev.*, 2019, **119**, 3349–3417.
12 T. J. Savenije, A. J. Ferguson, N. Kopidakis and G. Rumbles, *J. Phys. Chem. C*, 2013, **117**, 24085–24103.
13 H. Oga, A. Saeki, Y. Ogomi, S. Hayase and S. Seki, *J. Am. Chem. Soc.*, 2014, **136**, 13818–13825.
14 C. Wehrenfennig, G. E. Eperon, M. B. Johnston, H. J. Snaith and L. M. Herz, *Adv. Mater.*, 2014, **26**, 1584–1589.
15 A. Werner and M. Kunst, *Appl. Phys. Lett.*, 1985, **46**, 69–70.
16 R. J. O. M. Hoofman, M. P. de Haas, L. D. A. Siebbeles and J. M. Warman, *Nature*, 1998, **392**, 54–56.
17 T. J. Savenije, M. Nanu, J. Schoonman and A. Goossens, *J. Appl. Phys.*, 2007, **101**, 113718.

18 D. Friedrich and M. Kunst, *J. Phys. Chem. C*, 2011, **115**, 16657–16663.
19 F. F. Abdi, T. J. Savenije, M. M. May, B. Dam and R. van de Krol, *J. Phys. Chem. Lett.*, 2013, **4**, 2752–2757.
20 D. B. Straus, E. D. Goodwin, E. A. Gaulding, S. Muramoto, C. B. Murray and C. R. Kagan, *J. Phys. Chem. Lett.*, 2015, **6**, 4605–4609.
21 J. Park, O. G. Reid, J. L. Blackburn and G. Rumbles, *Nat. Commun.*, 2015, **6**, 8809.
22 E. A. Dolgopolova, A. J. Brandt, O. A. Ejegbavwo, A. S. Duke, T. D. Maddumapatabandi, R. P. Galhenage, B. W. Larson, O. G. Reid, S. C. Ammal, A. Heyden, M. Chandrashekhar, V. Stavila, D. A. Chen and N. B. Shustova, *J. Am. Chem. Soc.*, 2017, **139**, 5201–5209.
23 O. G. Reid, D. T. Moore, Z. Li, D. Zhao, Y. Yan, K. Zhu and G. Rumbles, *J. Phys. D: Appl. Phys.*, 2017, **50**, 493002.
24 A. Saeki, S. Seki, T. Takenobu, Y. Iwasa and S. Tagawa, *Adv. Mater.*, 2008, **20**, 920–923.
25 A. Crovetto, R. Nielsen, M. Pandey, L. Watts, J. G. Labram, M. Geisler, N. Stenger, K. W. Jacobsen, O. Hansen, B. Seger, I. Chorkendorff and P. C. K. Vesborg, *Chem. Mater.*, 2019, **31**, 3359–3369.
26 J. M. Warkan, P. D. Haas and A. Hummel, *Chem. Phys. Lett.*, 1973, **22**, 4.
27 J. M. Warman, M. P. de Haas, M. Grätzel and P. P. Infelta, *Nature*, 1984, **310**, 306–308.
28 M. P. de Haas, J. M. Warman, T. D. Anthopoulos and D. M. de Leeuw, *Adv. Funct. Mater.*, 2006, **16**, 2274–2280.
29 T. Okamoto, K. Nakahara, A. Saeki, S. Seki, J. H. Oh, H. B. Akkerman, Z. Bao and Y. Matsuo, *Chem. Mater.*, 2011, **23**, 1646–1649.
30 F. K.-C. Leung, F. Ishiwari, T. Kajitani, Y. Shoji, T. Hikima, M. Takata, A. Saeki, S. Seki, Y. M. A. Yamada and T. Fukushima, *J. Am. Chem. Soc.*, 2016, **138**, 11727–11733.
31 F. Zhang, D. H. Kim, H. Lu, J.-S. Park, B. W. Larson, J. Hu, L. Gao, C. Xiao, O. G. Reid, X. Chen, Q. Zhao, P. F. Ndione, J. J. Berry, W. You, A. Walsh, M. C. Beard and K. Zhu, *J. Am. Chem. Soc.*, 2019, **141**, 5972–5979.
32 M. J. Hong, S. R. Svadlenak, K. A. Goulas and J. G. Labram, *J. Phys. Mater.*, 2019, **3**, 014003.
33 M. J. Hong, R. Y. Johnson and J. G. Labram, *J. Phys. Chem. Lett.*, 2020, 4976–4983.
34 D. Weber, *Z. Naturforsch., B: J. Chem. Sci.*, 1978, **33**, 1443–1445.
35 N. J. Jeon, J. H. Noh, Y. C. Kim, W. S. Yang, S. Ryu and S. I. Seok, *Nat. Mater.*, 2014, **13**, 897–903.
36 S.-H. Turren-Cruz, A. Hagfeldt and M. Saliba, *Science*, 2018, **362**, 449–453.
37 M. Saliba, T. Matsui, J.-Y. Seo, K. Domanski, J.-P. Correa-Baena, M. K. Nazeeruddin, S. M. Zakeeruddin, W. Tress, A. Abate, A. Hagfeldt and M. Grätzel, *Energy Environ. Sci.*, 2016, **9**, 1989–1997.
38 D. P. McMeekin, G. Sadoughi, W. Rehman, G. E. Eperon, M. Saliba, M. T. Hörantner, A. Haghighirad, N. Sakai, L. Korte, B. Rech, M. B. Johnston, L. M. Herz and H. J. Snaith, *Science*, 2016, **351**, 151.
39 M. Kunst and G. Beck, *J. Appl. Phys.*, 1986, **60**, 3558–3566.
40 A. Miyata, A. Mitioglu, P. Plochocka, O. Portugall, J. T.-W. Wang, S. D. Stranks, H. J. Snaith and R. J. Nicholas, *Nat. Phys.*, 2015, **11**, 582–587.
41 K. Galkowski, A. Mitioglu, A. Miyata, P. Plochocka, O. Portugall, G. E. Eperon, J. T.-W. Wang, T. Stergiopoulos, S. D. Stranks, H. J. Snaith and R. J. Nicholas, *Energy Environ. Sci.*, 2016, **9**, 962–970.
42 M. E. Kamminga, H.-H. Fang, M. R. Filip, F. Giustino, J. Baas, G. R. Blake, M. A. Loi and T. T. M. Palstra, *Chem. Mater.*, 2016, **28**, 4554–4562.
43 R. Dingle, W. Wiegmann and C. H. Henry, *Phys. Rev. Lett.*, 1974, **33**, 827–830.
44 E. M. Hutter, M. C. Gélvez-Rueda, A. Osherov, V. Bulović, F. C. Grozema, S. D. Stranks and T. J. Savenije, *Nat. Mater.*, 2017, **16**, 115–120.
45 J. G. Labram and M. L. Chabinyc, *J. Appl. Phys.*, 2017, **122**, 065501.
46 E. M. Tennyson, T. A. S. Doherty and S. D. Stranks, *Nat. Rev. Mater.*, 2019, **4**, 573–587.
47 O. G. Reid, M. Yang, N. Kopidakis, K. Zhu and G. Rumbles, *ACS Energy Lett.*, 2016, **1**, 561–565.
48 P. P. Infelta, M. P. de Haas and J. M. Warman, *Radiat. Phys. Chem.*, 1977, **10**, 353–365.
49 M. P. De Haas and J. M. Warman, *Chem. Phys.*, 1982, **73**, 35–53.
50 H. Tsai, W. Nie, J.-C. Blancon, C. C. Stoumpos, R. Asadpour, B. Harutyunyan, A. J. Neukirch, R. Verduzco, J. J. Crochet, S. Tretiak, L. Pedesseau, J. Even, M. A. Alam, G. Gupta, J. Lou, P. M. Ajayan, M. J. Bedzyk, M. G. Kanatzidis and A. D. Mohite, *Nature*, 2016, **536**, 312–316.
51 N. R. Venkatesan, J. G. Labram and M. L. Chabinyc, *ACS Energy Lett.*, 2018, **3**, 380–386.
52 F. Zhang, H. Lu, J. Tong, J. J. Berry, M. C. Beard and K. Zhu, *Energy Environ. Sci.*, 2020, **13**, 1154–1186.
53 M. C. Fravventura, D. Deligiannis, J. M. Schins, L. D. A. Siebbeles and T. J. Savenije, *J. Phys. Chem. C*, 2013, **117**, 8032–8040.
54 A. Saeki, Y. Yasutani, H. Oga and S. Seki, *J. Phys. Chem. C*, 2014, **118**, 22561–22572.

